Molecular Dynamics Simulations of Barite and Celestite Ion-Pairs

A Thesis
Presented to
The Academic Faculty

By

Davis Morgan Warren

In Partial Fulfillment
of the Requirements for the Degree
Master of Science in Earth and Atmospheric Sciences

Georgia Institute of Technology

August, 2011

Molecular Dynamics Simulations of Barite and Celestite Ion-Pairs

Approved by:

Dr. Andrew G. Stack, Advisor
School of Earth and Atmospheric Sciences
Georgia Institute of Technology
and
Chemical Sciences Division
Oak Ridge National Lab

Dr. Ellery Ingall
School of Earth and Atmospheric Sciences
Georgia Institute of Technology

Dr. Philippe S. Van Cappellen
School of Earth and Atmospheric Sciences
Georgia Institute of Technology
and
Department of Earth and Environmental Sciences
University of Waterloo

Date Approved: June 27th, 2011

ACKNOWLEDGEMENTS

I would like to thank my family and friends for helping me not fall apart during this endeavor. A huge thanks goes to my advisor, Andrew Stack, for endless help in teaching me computational chemistry and for putting up with me. A special thanks to Meg Grantham and Jacky Bracco for words of encouragement and advice. I would also like to thank Paolo Raiteri of Curtin University (Australia) for the free energy perturbation code and Garret Thompson for assistance in writing the residence time correlation function program. I wish to thank my committee for scientific guidance and help with writing this thesis.

TABLE OF CONTENTS

LIST OF TABLES

LIST OF FIGURES

LIST OF SYMBOLS AND ABBREVIATIONS

A	Buckingham Constant (kcal mol^{-1})
A_{sc}	F3C Water Model Scaling Parameter
α	Degree of Dissociation
b	Bond Length (Å)
b_0	Equilibrium Bond Length (Å)
β	$1/k_BT$ ((kcal/mol)$^{-1}$)
C	Buckingham Constant (kcal mol^{-1}Å^6)
e	Fundamental Charge (1.602177 x 10^{-19} C)
ε_0	Permittivity of Free Space (8.854188 x 10^{-12} C^2 N^{-1} m^{-2})
ε	Van der Waals Potential Well Depth (kcal mol^{-1})
E	Ambient Thermal Energy (kcal mol^{-1})
F_i	Force Vector on Atom I (N)
f	WHAM Biasing Energy (kcal mol^{-1})
FEP	Free Energy Perturbation
fs	Femto-second (10^{-15} s)
ΔG_{hydr}	Hydration Free Energy (kcal mol^{-1})
$g(r)$	Radial Distribution Function (probability)
γ_{MX}	Activity Coefficient for Complex
$\gamma_{\pm}$	Mean Activity Coefficient
ΔH_{hydr}	Hydration Enthalpy (kcal mol^{-1})
K_i	Equilibrium Constant

K_A	Association Constant
K_C	Conditional Mass-Action Constant
k_{H2O}	Water Exchange Rate Constant (s^{-1})
k^{TST}	Transition State Theory Rate Constant (s^{-1})
k_B	Boltzmann Constant (0.001987 kcal mol^{-1} K^{-1})
k_b	Spring Constant (kcal mol^{-1} $Å^{-2}$)
k_a	Harmonic Angle Constant (kcal mol^{-1} $degrees^{-2}$)
k_t	Torsion Constant in Four-Body Potential (kcal mol^{-1})
κ	Transmission Coefficient
λ	WHAM Coupling Parameter
Λ	FEP Coupling Parameter
μ	Reduced Mass (kg)
m_i	Mass of Atom *i* (kg)
N	Number of Particles or Atoms
$n(x)$	Number of Counts in *x* number of Bins in Histogram
ns	Nano-second (10^{-9} s)
P	Pressure (atm)
$P(r)$	Probability Distribution
PMF	Potential of Mean Force (kcal mol^{-1})
ps	Pico-second (10^{-12} s)
q_i	Charge on atom *i* (C)
q_B	Bjerrum Length (Å)
QM/MM	Quantum Mechanics/Molecular Mechanics Simulation

r	Inter-Atom Separation Distance (Reaction Coordinate) (Å)
$r^{\ddagger}$	Transition State (Å)
r_i	Position Vector of Atom *i* (Å)
r_0	Equilibrium Separation Distance (Å)
ρ	Buckingham Constant (Å)
ρ_i	Number Density of Atom or Molecule *i* (atoms/volume)
T	Absolute Temperature (K)
t	Time (s)
τ	Water Residence Time (s^{-1})
θ	Bond Angle (degrees)
θ_0	Equilibrium Bond Angle (degrees)
$\theta(x)$	Heaviside Function
U	Potential Energy (kcal mol^{-1})
V	Volume ($Å^3$)
v_i	Velocity of Atom *i* (Å/fs)
WHAM	Weighted Histogram Analysis Method
$W(r)$	Potential of Mean Force (kcal mol^{-1})
$W(r)^{eff}$	Effective Potential of Mean Force (kcal mol^{-1})

SUMMARY

The presence of ion-pairs in electrolyte solutions affects the activity of dissolved species as well as the solubility of minerals. The extent of ion-pairing in a system is predicted by an association constant, K_A, which for sparingly soluble salts are frequently determined experimentally in binary or ternary systems. This introduces complex activity coefficient calculations that often require unavailable parameters. Barite ($BaSO_4$) and celestite ($SrSO_4$) are sparingly soluble minerals with interest in the oil and mining industry, yet the values of K_A for the ion-pairs $BaSO_{4(aq.)}$ and $SrSO_{4(aq.)}$ are still uncertain. Molecular dynamics simulations are used to obtain the K_A values for these two salts through potential of mean force (PMF) calculations. The molecular mechanisms involved in the association reactions are also explored, in particular the role of the association intermediates in the overall reaction as described by the Eigen mechanism. Additionally, the kinetics of water exchange around the free and paired ions is examined and the residence time of a water coordinated to the free and paired cation is calculated.

CHAPTER 1: INTRODUCTION

1.1 Motivation

The association of ions affects the behavior of electrolyte solutions by forming neutral as well as variably charged ion-pair species, hence altering long-range electrostatic interactions and lowering the activities of dissolved ions. This in turn affects the saturation index of minerals and their predicted solubility (Marcus, 1985; Drever, 1997). The degree of ion-pair formation increases with concentration, charge, and strength of hydration of the aqua species (Marcus, 1985) and as such becomes important in many natural (e.g. brines, cold seeps, hydrothermal vents, evaporite basins, oceans) and industrial (e.g. settling ponds, oil recovery, waste storage) settings where highly concentrated polyvalent solutions are present.

For example, a problem for oil companies has been the precipitation of barite ($BaSO_4$) and celestite ($SrSO_4$) scale in oil recovery pipes (Yuan et al., 1994). Seawater rich in sulfate (2700 ppm) (Hanor, 2000) is pumped into oil-bearing reservoirs, where it mixes with formation water rich in alkaline-earth metals, such as Ba^{2+} (780 ppm) and Sr^{2+} (78 ppm) (Hardy and Simm, 1996) creating a supersaturated solution, which induces scale precipitation. Precise determination of the concentration of $BaSO_{4(aq.)}$ and $SrSO_{4(aq.)}$ ion-pairs in the formation water would aid in predicting scale formation.

Another example can be found in studies on oceanic celestite in marine sediments. Equilibrium with celestite was found in 45 of 60 ODP drill cores, enough to warrant including this mineral in diagenetic models (Hoareau et al., 2010). Also, the concentration of Sr^{2+} in pore waters has been found to affect calcite ($CaCO_3$)

recrystallization rates (Richter, 1996); celestite equilibrium may provide a major constraint on the pore water Sr^{2+} concentration (Richter, 1996). Precisely knowing the concentration of $SrSO_{4(aq.)}$ ion-pairs in the pore-water will aid studies on carbonate recrystallization in ancient marine sediments and the global strontium budget (Richter, 1996; Hoareau et al., 2010).

Predicting the concentration of an ion-pair is done through the use of the association constant, K_A:

$$M^{m+}_{aq.} + X^{x-}_{aq.} \rightleftharpoons MX^{(m+x)}_{aq.} \tag{1.1}$$

$$K_A = \frac{[MX^{(m+x)}_{aq.}]\gamma_{MX}}{[M^{m+}_{aq.}][X^{x-}_{aq.}]\gamma_{\pm}^2} \tag{1.2}$$

where [] denotes concentration, γ is the activity coefficient (explained below), M is a cation, and X is an anion. Equation (1.1) is a simple association reaction that forms a complex and eq. (1.2) is the corresponding association constant. Unfortunately, the K_A values for $BaSO_{4(aq.)}$ and $SrSO_{4(aq.)}$ are not precisely known and conflicting values are reported in the literature (Monnin, 1999). For $BaSO_{4(aq.)}$ the reported $\log K_A$ values are 2.72 (Felmy et al., 1990) and 2.26 (Monnin, 1999) a difference of about a half an order of magnitude. For $SrSO_{4(aq.)}$, $\log K_A$ values of 1.86 (Felmy et al., 1990) and 2.29 are reported (Reardon & Armstrong, 1987), also a difference by about half an order of magnitude.

The conflicting values in K_A arise out of each mineral's low solubility and complications in activity coefficient calculations used in fitting the experimental data. The low solubility of barite ($\log K_{sp} = 10.05$) and celestite ($\log K_{sp} = 6.62$) keep ion-pair formation in pure water dissolution experiments negligible (Monnin, 1999). The common-ion effect is used to raise the minerals' solubility by dissolving the solid in a

solution composed of one of the solids' constituents; this increases the formation of ion-pairs making them easier to measure. Activity coefficients are used to account for the non-ideal effects inherent in electrolyte solutions resulting from the solutes interacting with each other. They are usually obtained from calculations based on specific properties of the chemical system. In the case of Pitzer's equations, these calculations require interaction parameters for barium and strontium that are not available. Hence, $CaSO_{4(aq.)}$ parameters are substituted in their place or set to zero (Felmy et al., 1990; Monnin, 1999).

Molecular dynamics (MD) simulation (see chapter 2 for details) provides an alternative to experimental methods for determining association constants. MD can be used to obtain equilibrium constants by calculating the change in free energy as ions associate (i.e. an energy surface). The energy surface along a reaction coordinate (the Cartesian distance between two ions in this case) can be computed as the potential of mean force (PMF). The PMF approach to obtain equilibrium constants for ion pairing reactions has been applied successfully to aqueous sodium chloride (Guárdia et al., 1991; Chialvo et al., 2003), alkaline-earth metal chloride complexes (Larentzos and Criscenti, 2008), divalent metal sulfate complexes (Matthews and Naidoo, 2010), divalent metal nitrate complexes (Xu et al., 2008), and divalent metal natural organic mater (NOM) complexes (Iskrenova-Tchoukova et al., 2010). Yet, to date no computational studies have been conducted on $BaSO_4$ and $SrSO_4$ aqueous ion-pairs.

MD also permits studying ion-association through the multi-step Eigen mechanism (Eigen and Tamm, 1964) (described in section 1.2). For strongly hydrated ions, such as Ba^{2+} and Sr^{2+}, multiple ion-pair species differing only by their degree of hydration may form during association (Marcus, 1985). These intermediates consist of

the ions separated by one or two waters and are called non-contact ion-pairs (non-CIP). These species are different than the contact ion-pair described in eq. (1.1) and may be important in accurately determining overall association constants (Buchner and Hefter, 2009). Alternative experimental methods for studying ion association (i.e. spectroscopic techniques, potentiometry, conductivity) can yield reliable association constants for simple association reactions such as exhibited in eq. (1.1). They are however less reliable for providing information on the intermediates involved in multi-step association processes (Hefter, 2006).

The goals of this thesis are to use PMF calculations to estimate the overall association constants, K_A, for $BaSO_{4(aq.)}$ and $SrSO_{4(aq.)}$ and investigate the role of the ion-pair intermediates in an association constant measurement. An additional study is conducted on the effect sulfate complexation has on the residence time of water in the first shell of each cation. The rate at which a molecule or ion exchanges its waters exerts a large control over its reactivity in solution, the effect of complexation on the residence time can shed light on the reactivity of these aqua complexes.

The method of Chialvo et al. (1995), also used by a number of other researchers (Larentzos and Criscenti, 2008; Matthews and Naidoo, 2010; Chialvo et al., 2003), will be used for determining the equilibrium constants. The Reactive Flux method (Chandler, 1978) will be used for the residence time calculations (Rey & Hines, 1996; Spångberg et al., 2003; Stack and Rustad, 2007). Subsequent residence time calculations will also be performed using the Residence Time Correlation Function (Impey et al., 1983) to compare to the Reactive Flux method.

Presented in this thesis is the first molecular dynamics study of the association reactions for $BaSO_{4(aq.)}$ and $SrSO_{4(aq.)}$ pairs through potential of mean force calculations. The first computational estimates of the overall association constants, K_A, as well as the equilibrium constants for the ion-pair intermediates, K_i, are presented. This will also be the first computational study exploring the effect sulfate complexation has on the water residence time for the cation in $BaSO_{4(aq.)}$ and $SrSO_{4(aq.)}$ pairs.

1.2 The Eigen Mechanism of Ionic Association

Ion association is studied in this thesis using the well-established (Pottel et al., 2007) multi-step Eigen mechanism (Eigen and Tamm, 1964). In this mechanism, fully solvated free aqua ions (FI) associate to form a solvent separated ion-pair (SSIP), where solvation shells remain intact and are separated by up to two waters:

$$[M^{m+}(OH_2)_n]_{FI} + [X^{x-}(H_2O)_n]_{FI} \rightleftharpoons [M^{m+}(OH_2)(OH_2)X^{x-}]_{SSIP} \quad (1.3)$$

Continued association penetrates the solvation shells forming a solvent shared ion-pair (SHIP), where both ions share a single water:

$$[M^{m+}(OH_2)(OH_2)X^{x-}]_{SSIP} \rightleftharpoons [M^{m+}(OH_2)X^{x-}]_{SHIP} \quad (1.4)$$

Further association expels the interior waters resulting in a contact ion-pair (CIP1):

$$[M^{m+}(OH_2)X^{x-}]_{SHIP} \rightleftharpoons [M^{\cdot\cdot}X^{(m+x)}]_{CIP1} \quad (1.5)$$

Depending on the nature of the anion and mass of the cation, a conformational rearrangement may result in a bidentate contact ion-pair (CIP2) (Burgess, 1999):

$$[M^{\cdot\cdot}X^{(m+x)}]_{CIP1} \rightleftharpoons [MX^{(m+x)}]_{CIP2} \quad (1.6)$$

An overall association constant can be written from the step-wise process using individual equilibrium constants by arranging eq. (1.3) through (1.6) as:

$$K_1 = \frac{[SSIP]}{[FI]} \quad (1.7a)$$

$$K_2 = \frac{[\text{SHIP}]}{[\text{SSIP}]} \tag{1.7b}$$

$$K_3 = \frac{[\text{CIP1}]}{[\text{SHIP}]} \tag{1.7c}$$

$$K_4 = \frac{[\text{CIP2}]}{[\text{CIP1}]} \tag{1.7d}$$

If we assume that:

$$[\text{MX}]=[\text{SSIP}]+[\text{SHIP}]+[\text{CIP1}]+[\text{CIP2}] \tag{1.8}$$

Equations (1.2) and (1.7a) through (1.7d) can be substituted into eq. (1.8) as:

$$K_A[\text{FI}] = K_1[\text{FI}] + K_2[\text{SSIP}] + K_3[\text{SHIP}] + K_4[\text{CIP1}] \tag{1.9}$$

Further substitution and elimination of variables yields:

$$K_A[\text{FI}] = K_1[\text{FI}] + K_1K_2[\text{FI}] + K_1K_2K_3[\text{FI}] + K_1K_2K_3K_4[\text{FI}] \tag{1.10}$$

and finally:

$$K_A = K_1 + K_1K_2 + K_1K_2K_3 + K_1K_2K_3K_4 \tag{1.11}$$

or

$$K_A = K_1(1 + K_2 + K_2K_3 + K_2K_3K_4) \tag{1.12}$$

Equation (1.12) is the final overall association constant used in the Eigen mechanism and is equivalent to eq. (1.2). The association constants reported in this thesis are calculated using eq. (1.12).

CHAPTER TWO: METHODS

2.1 Molecular Dynamics

Molecular dynamics is a computational method used to study the time evolution of a *N*-body system in a statistical ensemble to give a deterministic view of equilibrium and transport properties (Frenkel and Smit, 2002). Over the last several decades MD has become an integral part of theoretical (geo)chemistry and can guide experimentalists in new directions, as MD can allow insight into molecular level processes not easily observed through experiment (Frenkel and Smit, 2002). The MD method has gained widespread use in many disciplines of science: from physics, chemistry, material sciences, and biology (including medical applications such as pharmaceutical design and bioengineering) to the geologic sciences. This section briefly describes how molecular dynamics is performed including the forms of the equations used to predict the atomic interactions and some comments on statistical ensembles used in MD calculations.

2.1.1 Classical Molecular Dynamics

Classical molecular dynamics models the behavior of atoms using classical or Newtonian mechanics (Frenkel and Smit, 2002). This approach assumes that the atomic interactions being modeled can be done reasonably well without explicitly accounting for the electrons and molecular orbitals. Fortunately, this can be validated for most aqua ions because their behavior and dynamics is dominantly controlled by their hydration energy, charge, and mass (Richens, 1997; Collins et al., 2007). These quantities can be modeled accurately treating the atoms as point charges with an assigned mass and describing their interactions using classical physics.

In classical MD the motions of N particles (i.e. atoms) are described by:

$$r_i' = v_i \quad i = 1,2,3,...,N \tag{2.1}$$

$$F_i = m_i v_i' \quad i = 1,2,3,...,N \tag{2.2}$$

$$m_i v_i' = -\frac{\partial}{\partial r}\sum_{j=1}^{N} U_i(r_j) \quad i = 1,2,3,...,N \tag{2.3}$$

where r_i, is the position, v_i, is the velocity, m_i, is mass, F_i is the force, ' denotes a time derivative, and $U(\mathbf{r})$ is the total potential energy of the system and is described by a set of user-defined mathematical functions or "potentials" collectively called the force field (FF). The force field describes how the atoms interact through bond, angle, torsion, repulsion, and attraction terms in the mathematical functions (see section 2.2 for details on the force fields used in this study). Solving Newton's equations of motion for a N-body system becomes analytically impossible beyond $N = 3$, so the differential equations of motion are solved numerically. The velocity-Verlet algorithm is commonly used in many molecular dynamics software packages to solve the N-body problem. In this algorithm, time is discretized into individual "timesteps" and Taylor expansions are used to update the next positions and velocities of each atom at each time, t (Frenkel and Smit, 2002):

$$r_i(t + \Delta t) = r_i(t) + v_i(t)\Delta t + \frac{F(t)\Delta t^2}{2m_i} \tag{2.4}$$

$$v_i(t + \Delta t) = v_i(t) + \frac{F(t + \Delta t) + F(t)\Delta t}{2m_i} \tag{2.5}$$

where $r_i(t)$, $v_i(t)$, and $F_i(t)$, is the position, velocity and force vectors of atom, i, at time, t, and m_i is the mass. The velocity-Verlet algorithm is calculated in three consecutive steps;

first the new positions are updated; from this the new velocities can be calculated, followed by the new forces. Each timestep provides a snapshot from which the ensemble statistics are averaged and calculated.

2.1.2 Statistical Ensembles

Statistical mechanics relate the microscopic properties and motions of atoms to macroscopic observable thermodynamic quantities (e.g. Pressure, Volume, Temperature). Central to statistical mechanics, and thus MD, is the postulation that the average value of a calculated mechanical property, $\langle P \rangle$, equals the same observed equilibrium thermodynamic quantity, P_{obs}, where brackets denote an ensemble average. An ensemble is the assembly of all possible microstates (i.e. configurations of the system) available with given constraints (Chandler, 1987), the constraints being the fixed independent thermodynamic variables, which then define the ensemble. Two ensembles are used in this thesis, the canonical (fixed number of particles, *N*, volume, *V*, and temperature, *T*) and the isothermal-isobaric (fixed number of particles, *N*, pressure, *P*, and temperature, *T*) ensembles. A two-stage equilibration process was used where the system is initially run in the isothermal-isobaric ensemble to achieve an equilibrium volume for the system and then the canonical ensemble is run with the volume fixed at the equilibrium value. This ensures the computed quantities are from equilibrium configurations consistent with the physically relevant pressure and temperature of the system being modeled.

2.2 The Force Fields

The quality of an MD simulation is critically dependent on how accurately the FF describes the atomic interactions. Often, a classical molecular dynamics FF is fit to

structures calculated from *ab initio* techniques (i.e. DFT, Hartree-Fock) (Cygan, 2001) and further calibrated to produce experimental free energies. In this study the force fields used were the F3C water model (Levitt et al., 1993), a modified (Stack and Rustad, 2007; Stack, 2009) version of the MSXX barite model (Jang et al., 2002), and a modified version of the MSXX celestite model (Jang et al., 2002). Below is a description of the potentials used in each model.

2.2.1 Flexible Three Centered Water Model

The flexible three centered water (F3C) model (Levitt et al., 1997) was originally developed to aid in the simulation of biological macromolecules. The design philosophy of the F3C water model is as follows: it only considers the atoms as point charges, does not fix bond lengths or angles (helping to preserve the dynamic nature of liquid water), and includes Van der Waals interactions for the hydrogen atoms. Van der Waals interactions on the hydrogens is a unique feature of the F3C water model. One of the principle reasons for using this model was to account for the effects of the hydrogen-bonds on the barium, strontium, and sulfate ions (Jang et al., 2002).

The F3C water model considers the following contributions to its total potential energy (Levitt et al., 1997):

$$U_{total} = U_{bond} + U_{angles} + U_{non-bonded} + U_{Coulombic} \tag{2.6}$$

The bonds are described as harmonic springs, where b is the bond length, b_0 is the equilibrium bond length, and k_b is the force constant:

$$U_{\text{bond}} = \sum_{i=1}^{N_{bonds}} \tfrac{1}{2} k_b (b - b_0)^2 \tag{2.7}$$

The angles are described by a harmonic angle equation, where θ is the bond angle, θ_0 is the equilibrium bond angle, and k_a is the force constant:

$$U_{\text{angles}} = \sum_{i=1}^{N_{angles}} \tfrac{1}{2} k_a (\theta - \theta_0)^2 \tag{2.8}$$

The non-bonded Van der Waals interactions are described using a scaled Lennard-Jones style equation, where A_{sc} is the scaling parameter, ε is the well depth in the potential energy function, r_{ij} is the separation distance between two atoms i and j, and r_0, is the equilibrium separation distance between two atoms i and j:

$$U_{\text{non-bonded}} = \sum_{i=1}^{N_{vdW}} \left[A_{sc} \varepsilon \left(r_0 / r_{ij} \right)^{12} - 2\varepsilon \left(r_0 / r_{ij} \right)^{6} \right] \tag{2.9}$$

The electrostatic interactions are described using Coulomb's law, where e is the fundamental charge, ε_0 is the dielectric constant, q_i is the charge on atom i, and r_{ij} separation distance between atoms i and j:

$$U_{\text{Coulombic}} = \frac{e^2}{4\pi\varepsilon_0} \sum_{i \neq j} \frac{q_i q_j}{r_{ij}} \tag{2.10}$$

The F3C water model has been calibrated to reproduce the structure, hydration enthalpy, diffusion coefficient, and heat capacity of water as determined by experiment and was found to do so adequately (Levitt et al., 1997). Unfortunately no value was reported for the model's dielectric constant. Values of the constants used in the F3C water model can be found in Table 2.1.

Table 2.1 - Constants for F3C water model (after Levitt et al., 1997)

Bonded Interactions				
U_{bonds}	k_b (kcal/mol/Å^2)	250	r_0 (Å)	1.00
U_{angles}	k_a (kcal/mol/rad^2)	60	θ_0 (°)	109.47
Non-Bonded Interactions				
U_{VdW}		ε (kcal/mol)	r_0 (Å)	A_{sc}
	O_w-O_w	0.1848	3.5532	1
	O_w-H	0.043	1.7883	1
	H-H	0.01	0.9	1
Coulombic				
q	O_w	-0.82|*e*|		
	H	+0.41|*e*|		

O_w is the oxygens on water, H is the hydrogens

2.2.2 MSXX Barite/Celestite Model

The MSXX model (Jang et al. 2003; Stack & Rustad 2007; Stack, 2009) was designed to be implemented with the F3C water model in order to simulate growth morphology and the mineral-water interface. The model has been calibrated to cell parameters, hydration and lattice enthalpies, experimental compressibility, and frequencies of internal vibration modes, as well as solvent structures of the lattice ions (Jang et al., 2002). In an effort to make the model more portable, Stack and Rustad (2007) calibrated the non-bonded Ba-SO_4-H_2O interactions to a Buckingham-style equation.

The MSXX force field considers the following contributions to the total potential energy:

$$U_{total} = U_{bond} + U_{angles} + U_{torison} + U_{non-bonded} + U_{Coulombic} \quad (2.11)$$

The bonds are described as harmonic springs, where b is the bond length, b_0 is the equilibrium bond length, and k_b is the force constant:

$$U_{\text{bond}} = \sum_{i=1}^{N_{bonds}} \tfrac{1}{2} k_b (b - b_0)^2 \tag{2.7}$$

The angles are described by a harmonic cosine three-body angle equation (Mayo et al., 1990), where θ is the angle, θ_0 is the equilibrium angle, and k_a is the force constant:

$$U_{angles} = \sum_{i=1}^{N_{angles}} \frac{k_a}{2\sin^2\theta_0}\left(\cos\theta - \cos\theta_0\right)^2 \tag{2.12}$$

The four-body interactions of the sulfate molecule are described by a harmonic cosine four-body equation, where θ_{01} and θ_{02} are the equilibrium angles in the torsion bend; θ_1 and θ_2 are the angles in the torsion bend. This term is used to maintain the geometry of the sulfate molecule as well as account for the energy arising from the torsion bends:

$$U_{torsion} = \sum_{i=1}^{N_{torsion}} \frac{k_t}{\sin\theta_{0_1}\sin\theta_{0_2}}\left(\cos\theta - \cos\theta_{0_1}\right)\left(\cos\theta - \cos\theta_{0_2}\right)^2 \tag{2.13}$$

The non-bonded Van der Waals interactions are described by a Buckingham equation where A, ρ, and C are constants and r_{ij} is the separation distance between atoms i and j, with the first term describing the attractive forces and second term describing the repulsive forces:

$$U_{non-bonded} = \sum_{i=1}^{N_{vdW}} \left[A e^{-r/\rho} - \frac{C}{r^6} \right] \tag{2.14}$$

The electrostatic interactions are described using Coulomb's law, where e is the elementary charge, ε_0 is the dielectric constant, q_i is the charge on atom i, and r_{ij} is the separation distance between atoms i and j:

$$U_{\text{Coulombic}} = \frac{e^2}{4\pi\varepsilon_0} \sum_{i \neq j} \frac{q_i q_j}{r_{ij}} \tag{2.10}$$

The modifications made to the celestite MSXX model were to fit the Sr-H_2O non-bonded interactions to a Buckingham-style equation, hence making them more portable (This Study). The modifications were calibrated to experimental solvation structures and hydration enthalpies (see section 2.7) (Hofer et al., 2006; Richens, 1997). The strontium-sulfate interactions were derived from standard combination rules using a geometric mean for the *A* and *C* constants and an arithmetic mean for ρ (This Study). Values of the constants used in the MSXX force field can be found in Table 2.2.

Table 2.2 - Constants for Barite/Celestite Ion-Pair Force Field

Bonded Interactions[1,2,3]						
U_{bonds}	k_b (kcal/mol/Å^2)	477.5	r_0 (Å)	1.505		
U_{angles}	k_a (kcal/mol/rad^2)	196.87	θ_0 (°)	109.47		
$U_{torsion}$	k_a (kcal/mol/rad)	80.6	θ_{01} (°)	109.47	θ_{02} (°)	109.47
U_{bb}	k_{bb} (kcal/mol/Å^2)	102	r_0 (Å)	1.505		

Non-Bonded Interactions[2,3]				
U_{vdW}		A (kcal/mol)	ρ (Å)	C (kcal/mol/Å^6)
	S-S	55988	0.33583	2947
	S-O_s	55491	0.29417	890
	S-O_w	62638	0.30458	1427
	S-H	12426	0.29694	274
	O_s-O_s	5000	0.25251	269
	O_s-H	12316	0.25528	82.6
	O_s-O_w	58931	0.27308	269
	Ba-O_w	118150	0.29588	3036.5
	Ba-H	13902	0.173003	3.96
	Ba-S	46412	0.34666	762
	Ba-O_s	46000	0.305	230
	Ba-Ba	38473	0.35749	197
	Sr-O_w[4]	1030238	0.22065	1800
	Sr-H[4]	35900	0.211	15.4
	Sr-S[4]	35151	0.35201	893
	Sr-O_s[4]	34848	0.31035	270
	Sr-Sr[4]	22070	0.3682	271

Coulombic[1]		
q	S	+1.544|*e*|
	O_s	-0.866|*e*|
	Ba	+2.00|*e*|
	Sr	+2.00|e|

O_w is oxygen on water, O_s is oxygen on sulfate, S is sulfur, and H is hydrogen
[1]Jang et al., 2002. [2]Stack and Rustad, 2007. [3]Stack, 2009. [4]This Study.

2.3 Simulation Details – The Water Box

Molecular dynamics calculations were performed with the LAMMPS software package (Plimpton, 1995). Free ion calculations were performed in a 20 x 20 x 20 Å box

with 267 water molecules (0.99 g/cc) and 1 ion (barium, strontium, or sulfate), corresponding to an aqueous concentration of 0.207 M. Ion-pairing calculations were performed in a 41 x 41 x 41 Å box containing 2307 water molecules (1.00 g/cc), 1 SO_4^{2-}, and 1 cation, corresponding to an aqueous concentration of 0.024 M. The canonical (NVT) ensemble was used for all final calculations averaged over 1 ns of MD time preceded by a 100 ps equilibration period in the isothermal-isobaric ensemble (NPT). All simulations were performed at 300 K and 1 atm.

2.4 Potential of Mean Force Calculations

The PMF or $W(r_{ij})$, between two atoms, *i* and *j*, (e.g. a cation and an anion in an ion pair) along a reaction coordinate, *r*, represents the change in free energy arising from the interaction between atoms *i* and *j* at a fixed distance, r_{ij}, while the remaining molecules are averaged over all configurations sampled by the system (McQuarrie, 1976). When atoms *i* and *j* are in a solvent, $W(r_{ij})$ will include the free energy contributions of the solvent and of *i* and *j* on each other (Ghoufi and Malfreyt, 2006). As a result the calculation of the PMF has become central to computational and statistical mechanical studies of chemical reactions in liquids (Roux, 1995). In this thesis the PMF is computed in two different ways, described below.

2.4.1 Radial Distribution Function

For reactions with a small activation energy relative to the ambient thermal energy of the system, $E = k_B T$, where k_B is Boltzmann's constant and T is the absolute temperature, the probability of the system sampling all states along the reaction coordinate are high enough that the PMF can be generated from the radial distribution function, $g(r)$ (Chandler, 1987):

$$W(r) = -\beta \ln(g(r)) \tag{2.15}$$

where, $\beta = 1/k_B T$. The radial distribution function indicates how the probability (or number density) changes as a function of the atom-atom distance, r. In other words it shows at what distance from each other the atoms are most likely to be. This definition assumes the reaction coordinate is rectilinear and that the dynamical contributions to the energy surface are correctly modeled using a linear combination of Cartesian coordinates. This assumption is not valid for reactions in solution and a correction is applied to account for the curvilinear nature of the coordinate, hence creating a solvent averaged effective potential, $W(r)^{eff}$ (Schenter et al., 2003; Spångberg et al., 2003):

$$W(r)^{eff} = W(r) - 2\beta^{-1} \ln\left(\frac{r}{r^{\ddagger}}\right) \tag{2.16}$$

where $r^{\ddagger}$ is the dividing point (i.e. the maximum in $W(r)$) along the reaction coordinate (Figure 2.1). This correction will be applied to all free energy profiles generated in this thesis.

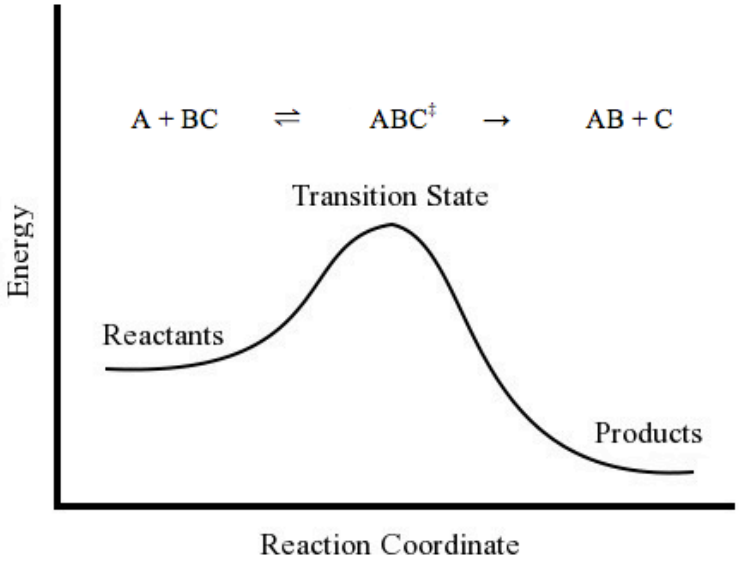

Figure 2.1 - Schematic of potential of mean force, showing location of a transition state.

2.4.2 Weighted Histogram Analysis Method (WHAM)

For reactions with higher activation energies, roughly twice ambient thermal energy, the probability of the system sampling all states along the reaction coordinate diminishes. Therefore, a statistically meaningful interpretation of the data cannot be achieved in a reasonable amount of simulation time, which is usually on the order of femtoseconds to nanoseconds. To put it another way, the reaction will never leave the stable reactants side of the coordinate to yield products (Figure 2.1). To obtain adequate sampling of all states in the system the reaction needs to be "pushed" or biased along the coordinate. The Weighted Histogram Analysis Method (WHAM) (Kumar et al., 1992) provides an efficient method to bias the reaction and obtain the PMF.

In WHAM, *W(r)* is calculated by a linear combination of weighted (biased) histograms, representing the probability, *P(r)* (in this case *g(r)*), at each point along the

reaction coordinate, *r*. The energy of the bias used to push the sampling is removed and the PMF is computed at each point along the reaction coordinate by iteratively solving the WHAM equations until convergence:

$$P(U_{bias},r) = \frac{\sum_{\lambda=1}^{N} n_{\lambda}(r)}{\sum_{\lambda=1}^{N} N_{\lambda} e^{-\beta(U_{bias} - f_{\lambda})}} \tag{2.17}$$

$$f_{\lambda} = -\beta^{-1} \ln\left(\sum_{x} P(U_{bias},r) e^{-\beta U_{bias}(r)} \right) \tag{2.18}$$

where $P(U_{bias},r)$ is the probability distribution, $\beta = 1/k_B T$, N is the number of simulations, x is the number of histogram bins, $n_{\lambda}(r)$ is the number of counts in each histogram bin, U_{bias} is the biasing potential (a harmonic spring in this case), λ is the coupling parameter (position on the reaction coordinate), and f_{λ} is the energy of introducing the bias for each value of λ. The probability distribution is computed as a histogram centered on each value of λ, the bias potential, U_{bias}, holds the system at λ to create the biased sampling. All WHAM calculations in this thesis are performed with Alan Grossfield's WHAM program (Grossfield, unpublished, http://dasher.wustl.edu/alan/wham, accessed 6/23/2007).

2.5 Association Constants from the Potential of Mean Force

The method of Chialvo et al. (1995) is used to compute the association constants from the PMF profiles. This method has been used successfully by other researchers (Larentzos and Criscenti, 2008; Matthews and Naidoo, 2010; Iskrenova-Tchoukova et al., 2010) and presents a straightforward methodology for arriving at an association constant from the PMF profile. The following is from Chialvo et al., (1995).

Starting with the Eigen mechanism association constant from section 1.2:

$$K_A = K_1(1 + K_2 + K_2K_3 + K_2K_3K_4) = \frac{[\mathrm{MX}]\gamma_{\mathrm{MX}}}{[\mathrm{M}][\mathrm{X}]\gamma_{\pm}^2} \tag{2.19}$$

where M is a cation, X is an anion, γ_{MX} is the activity coefficient for the complex, and $\gamma_{\pm}$ is the mean activity coefficient for free ions. Equation (2.19) is rewritten in terms of the degree of dissociation, α:

$$K_A = \frac{(1-\alpha)\gamma_{\mathrm{MX}}}{c\alpha^2\gamma_{\pm}^2} \tag{2.20}$$

where c is the molal concentration. Alternatively, eq. (2.20) may be written in terms of a conditional mass-action constant, K_C:

$$K_A = K_C \frac{\gamma_{\mathrm{MX}}}{\gamma_{\pm}^2} \tag{2.21}$$

K_C can then be expressed in terms of the number densities (number of atoms/volume) of the different solutes as:

$$K_C = \frac{\rho_{MX}}{\rho_M \rho_X} = \frac{(1-\alpha)}{\rho_0\alpha^2} \tag{2.22}$$

where ρ_{MX} is the number density of the CIP, ρ_M is the number density of the cations, ρ_X is the number density of the anions, and ρ_0 is the total number density of all species. The number density can be represented by the statistical mechanical anion-to-cation radial distribution function, $g_{MX}(r)$, when the inter-nuclear separation distance, r, is within the upper and lower bounds of integration, r_U and r_L, respectively (Cummings and Stell, 1984):

$$\rho_{MX} = 4\pi\rho_0^2 \int_{r_L}^{r_U} g_{MX}(r) r^2 dr \tag{2.23}$$

Similarly the degree of dissociation can be written as:

$$(1-\alpha) = 4\pi\rho_0 \int_{r_L}^{r_U} g_{MX}(r) r^2 dr \tag{2.24}$$

Combining eq. (2.19) through (2.24), an expression for the statistical-mechanical association constant is:

$$K_A = \frac{4\pi\gamma_{MX}\gamma_{\pm}^{-2}\int_{r_L}^{r_U} g_{MX}(r) r^2 dr}{\left(1 - 4\pi\rho_0 \int_{r_L}^{r_U} g_{MX}(r) r^2 dr\right)^2} \tag{2.25}$$

Assuming infinite dilution, where $K_A = K_C$ and the activity coefficients are $\gamma_{MX} = \gamma_M = \gamma_X = 1$; the final expression may be written as:

$$K_A = 4\pi \int_{r_L}^{r_U} g_{MX}^{\infty}(r) r^2 dr \tag{2.26}$$

Using eq. (2.15) and (2.16), eq. (2.26) is rewritten in terms of the effective PMF, $W(r)^{eff}$:

$$K_A = 4\pi \int_{r_L}^{r_U} e^{-\beta W(r)^{eff}} dr \tag{2.27}$$

The same methodology that arrived at eq. (2.27) can be used for the individual equilibria in the Eigen mechanism; rewriting eq. (1.7a) to (1.7d) we arrive at:

$$K_1 = \frac{[\text{SSIP}]}{[\text{FI}]} = \frac{\int_{r_3}^{r_4} e^{-\beta W(r)^{eff}} dr}{\int_{r_4}^{r_n} e^{-\beta W(r)^{eff}} dr} \tag{2.28a}$$

$$K_2 = \frac{[\text{SHIP}]}{[\text{SSIP}]} = \frac{\int_{r_2}^{r_3} e^{-\beta W(r)^{eff}} dr}{\int_{r_3}^{r_4} e^{-\beta W(r)^{eff}} dr} \tag{2.28b}$$

$$K_3 = \frac{[\text{CIP1}]}{[\text{SHIP}]} = \frac{\int_{r_1}^{r_2} e^{-\beta W(r)^{eff}} dr}{\int_{r_2}^{r_3} e^{-\beta W(r)^{eff}} dr} \tag{2.28c}$$

$$K_4 = \frac{[\text{CIP2}]}{[\text{CIP1}]} = \frac{\int_{0}^{r_1} e^{-\beta W(r)^{eff}} dr}{\int_{r_1}^{r_2} e^{-\beta W(r)^{eff}} dr} \tag{2.28d}$$

Where the bounds of integration are the successive peaks in the PMF (i.e. r_1 is the first peak, etc.). Equation (1.12) is then calculated using eq. (2.28a) through (2.28d) creating an expression for calculating the overall association constant from the PMF profile.

2.6 Water Residence Times from the Potential of Mean Force

The fundamental reactivity of an ion in water is controlled by its water exchange rate, k_{H2O} (Richens, 1997). For a first-order reaction, the residence time, τ, is equal to the inverse of the first-order water exchange rate, k_{H2O}: $\tau = 1/k_{H2O}$. The residence time is then defined as the average amount of time a particular water molecule spends coordinating an ion before entering bulk water. These quantities can be used to help understand the molecular mechanisms of chemical reactions. The residence time is calculated using two methods in this thesis; Reactive Flux (Chandler, 1978) and the residence time correlation function (Impey et al., 1983).

2.6.1 Reactive Flux

The Reactive Flux (RF) method (Chandler, 1978) is used to calculate an exact first-order water exchange rate constant from the product of the transition state theory rate constant, k^{TST}, and a time-dependent transmission coefficient, κ: $k_{H2O} = k^{TST}\kappa$. Transition state theory assumes that there is a saddle point, $r^{\ddagger}$, on the potential energy surface (i.e. the PMF) that represents a dividing point for the reaction coordinate separating reactants from products. This corresponding energy state is the transition state (Figure 2.1); that according to the theory, every elementary reaction must proceed through to become products (Eyring, 1935; Wigner, 1938).

A rate may be calculated from the PMF once the transition state has been defined (Wigner, 1938; Chandler, 1978; Rey and Hynes, 1996):

$$k^{TST} = \sqrt{\frac{1}{2\pi\mu\beta}} \frac{r^{\ddagger 2} e^{-\beta W(r^{\ddagger})}}{\int_0^{r^{\ddagger}} r^2 e^{-\beta W(r)} dr} \tag{2.29}$$

where the equation represents the probability of the reactants reaching the transition state, $r^{\ddagger}$, normalized by the integral of all possible reactant state probabilities. Equation (2.29) assumes that 100 % of the molecules reaching the transition state will cross to products or $\kappa = 1$ (Eyring, 1935; Wigner, 1938; Chandler 1978).

The transmission coefficient takes into account the solvents ability to cause molecules to recross on the dividing point:

$$\kappa = \frac{\left\langle \delta\left[r(0) - r^{\ddagger}\right] \dot{r}(0) \theta\left[r(t) - r^{\ddagger}\right] \right\rangle}{\left\langle \delta\left[r(0) - r^{\ddagger}\right] \dot{r}(0) \theta\left[\dot{r}(0)\right] \right\rangle} \tag{2.30}$$

where *r(t)* is the reaction coordinate at time, *t*, θ is the Heaviside function and equals one if the configuration is in a product state or zero if in a reactant state, δ is the derivative of θ, and $\dot{r}$ refers to the derivative of the position (i.e. the velocity). The numerator is the average in phase space over all configurations in the product state at time, *t*. The denominator is the velocity weighted average of all configurations going towards products at time, *t*. As κ evolves with time it will plateau when the amount of barrier recrossings become steady, this plateau value is κ.

The transmission coefficient was calculated by running an initial 10 ns simulation with the system held in the transition state by the SHAKE algorithm (Ryckaert et al., 1985). During the 10 ns simulation, configurations were harvested and used to create 2000 simulations that all started at the transition state. These new simulations were assigned random Boltzmann velocities to create unique runs. Each new transition state structure was then run forward and backward for 2 ps while κ was calculated, this

provides a way to asses the solvents affect on how the reaction progresses from the chosen transition state.

2.6.2 Residence Time Correlation Function

Impey et al. (1983) developed what has been termed a 'direct sampling' approach for obtaining the residence time. This method is attractive because it does not require knowledge of the transition state or the computation of a potential of mean force. All that is required is the distance to the first water shell around the aqua ion of interest, which can be readily obtained from the *g(r)*. A step function, *R(t)*, was used to count the coordinated waters as a function of time:

$$R(t) = \left\langle \frac{1}{N_0} \sum_{i=1}^{N_t} \theta_i(0)\theta_i(t) \right\rangle \tag{2.31}$$

where N_t is the number of waters coordinated at time, t; $\theta(t)$ is the Heaviside function, which is zero if the water molecule of interest, i, is not coordinated and one if the water is coordinated. A tolerance time of 2 ps is used to allow for molecular mobility of the waters, meaning a water is only counted as having left the shell if it has done so for more than the tolerance time. This tolerance time of 2 ps is used; out of convention (Impey et al., 1982; Kerisit and Rosso, 2009; Larentzos and Criscenti, 2008), but also because studies have shown that it takes about 2 ps for a water molecule to diffuse from the first to the second shell (Impey et al., 1983). The water exchange rate is then extracted by fitting the *R(t)* function to an exponential decay, $R(t) \sim \exp(-k_{H2O}t)$. The disadvantage of this approach is that the fit can sometimes be arbitrary.

2.7 Energy Calculations

In order to compare computational results to experimental values, careful attention must be paid to thermodynamic quantities so that the modeled system has

energetics consistent with the real experimental system. The hydration enthalpy, ΔH_{hydr}, and free energy, ΔG_{hydr}, were used for the comparisons in this thesis. Two methods were used to calculate the hydration energies for the ions: one, a simple subtraction scheme and two, the free energy perturbation (FEP) method. Unless otherwise noted all reported energies are from the subtraction method.

2.7.1 Subtraction Method

A simple subtraction scheme was used to calculate the hydration energy of the ions:

$$U_{H2O} - U_{H2O+X} = U_X \tag{2.32}$$

where U_{H2O} is the total potential energy of bulk water, U_{H2O+X} is the total potential energy of bulk water with an added ion, and U_X is the potential energy of the ion (where X = Ba^{2+}, Sr^{2+}, or SO_4^{2-}). The modified force fields for celestite and barite (Stack and Rustad, 2007; Stack, 2009) are calibrated in this way, by comparing the difference in potential energy to the experimental hydration enthalpy. During the course of the research it was identified that this approach has an inherent problem, the subtraction technique does not completely sample all states of the system that contribute to the free energy solvation. Using a Hamiltonian (operator for the potential energy of the system) modified with a coupling parameter solves this problem by calculating the free energy difference in stages obtaining a complete description of all the states in the solvation process. Free energy perturbation calculates free energies in just this way.

2.7.2 Free Energy Perturbation

In free energy perturbation (FEP) theory the Gibbs free energy of hydration is calculated by making an ion appear or disappear in the solvent by gradually switching off

and back on again the interactions of the ion with the solvent (Chipot and Pohorille, 2007). This overcomes the inaccuracies inherent in the subtraction technique by using the same Hamiltonian for both the reference and the final state ensuring that all the states of the system are sampled. A coupling parameter, Λ, was added to the Hamiltonian and used to gradually switch from the reference (Λ=0) to the final (Λ=1) state in stages. The difference in potential energy of the final and reference system was calculated for each value of Λ:

$$\Delta G = -\frac{1}{\beta}\sum_{i=1}^{N-1}\ln\left\langle \exp\left[-\beta(U(\Lambda_{i+1}) - U(\Lambda_i))\right]\right\rangle_{\Lambda_i} \tag{2.33}$$

Where ΔG is the hydration free energy, $\beta = 1/k_B T$, U is the potential energy, Λ is the coupling parameter, and $\langle \ldots \rangle$ denotes an ensemble average. The calculation was performed in a modified version of the DL_POLY 2.19 software package (Smith and Forester, 1996; P. Raiteri, pers. comm.). The calculations were split in to the electrostatic and Van der Waals terms to aid in convergence and final calculations were run for 2 ns with a 50 ps equilibration time.

CHAPTER 3: RESULTS & DISCUSSION

3.1 Hydration Structure and Energy

Calculated hydration energies and structures are summarized in Table 3.1. Using the F3C water model (Levitt et al., 1997) the hydration enthalpy, ΔH_{hydr}, of bulk water is -41.4 kJ/mol; which compares well to the experimental value of -41.5 kJ/mol. The first maximum in the O_w-O_w radial distribution function, $r_{O\text{-}O}$, occurrs at 277pm, somewhat shorter than the value obtained from neutron diffraction of 288 pm for $r_{O\text{-}O}$. The peak height (i.e. the probability of finding a water at a O_w-O_w distance) of F3C water is 3.04, whereas the neutron diffraction peak height is 3.09 for *g(r)* (Soper, 1986). The F3C water coordination number (CN) is 4.5 waters, in good agreement with a QM/MM study, 4.1 (Hofer et al., 2004), and the value of 4.8 reported by Marcus (1985).

The calculated ΔH_{hydr} of aqueous Ba^{2+} ion is -1373 kJ/mol, 5.2 % more negative than the experimental value of -1305 kJ/mol (Persson et al., 1995), and 5.5 % more negative than the previous implementation of this FF (Stack, 2009), which results from using a different system size. The calculated $r_{Ba\text{-}O}$ is 276 pm coordinated by 8.7 waters (Figure 3.1). These values compare well with recent QM/MM results (Hofer, 2005), which yielded 286 pm and 8.8 for $r_{Ba\text{-}O}$ and the CN respectively, and to an EXAFS study (Persson, 1995) that yielded 282 pm for $r_{Ba\text{-}O}$ and 8.1 for the CN.

The calculated ΔH_{hydr} of aqueous Sr^{2+} ion is -1468 kJ/mol, 0.5 % more negative than the reported value of -1443 kJ/mol (Persson, 1995). The calculated $r_{Sr\text{-}O}$ is 261 pm coordinated by 8.3 waters (Figure 3.1). This matches EXAFS results (Parkman et al., 1998) of 262 pm and 8.3 for $r_{Sr\text{-}O}$ and CN, respectively. More recent QM/MM studies

(Hofer et al., 2006) of Sr^{2+} have yielded higher values of 269 pm and 9.0 for $r_{Sr\text{-}O}$ and CN, respectively. Although the modifications to the strontium FF were made to fit to these values, they are reported here with the results of the other force fields for consistency.

The calculated ΔH_{hydr} of aqueous SO_4^{2-} ion is -1044 kJ/mol, 5.7 % less negative than the experimental value of -1108 kJ/mol (Marcus, 1985) and 4.7 % less negative than the previous implementation of this FF (Stack, 2009), which as previously stated results from using a different system size. The calculated $r_{S\text{-}O}$ is 394 pm coordinated by 15.8 waters. The average S-O distance is not well-constrained and reported values range from 362 pm from LAXS (Vchirawongkwin et al., 2007), 393 pm from XRD (Ohtaki, 1993), and 383 pm from QM/MM (Vchirawongkwin et al., 2007), reported CN for aqueous sulfate range from 8-14 for a QM/MM study and 12 from LAXS (Vchirawongkwin et al., 2007). Our results for the S-O distance and CN are at the upper limit of reported values.

Table 3.1: Calculated Hydration Structure and Energy for Aqueous Species and Water

		This Study	Lit. Values	Reference
Ba^{2+}	Ba-O_w (pm)	276	278-290	Hofer et al., 2005; Ohtaki, 1993
	CN	8.7	9.3,8.1	Hofer et al., 2005; Richens, 1996
	ΔH (kJ/mol)	-1373	-1305	Richens, 1996
Sr^{2+}	Sr-O_w (pm)	261	260-269	Hofer et al., 2006; Ohtaki, 1993
	CN	8.3	8.3	Hofer et al., 2006
	ΔH (kJ/mol)	-1468	1476, 1443	Vasilev, 1960; Richens, 1996
SO_4^{2-}	S-O_w (pm)	394	361-393	Vchirawongkwin, 2007; Ohtaki, 1993
	CN	15.8	8-14,12	Vchirawongkwin, 2007
	ΔH (kJ/mol)	-1044	-1108	Persson, 1995
H_2O	O_w-O_w (pm)	277	288	Soper, 1986
	CN	4.5	4.8	Marcus, 1985
	ΔH (kJ/mol)	-41.4	-41.5	Marcus, 1985

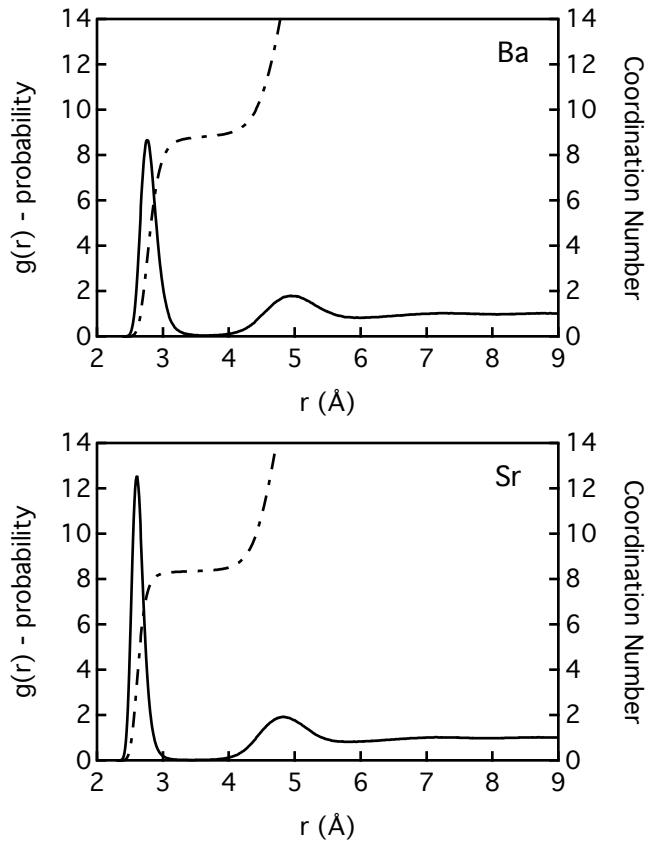

Figure 3.1 Radial distribution functions and coordination numbers for M-O_w pairs (M = Ba(II), Sr(II). Solid line is the g(r) ploted along the left axis, dashed line is the CN plotted against the right axis.

A simple subtraction method (see Section 2.7) of calibrating the hydration enthalpies was found to depend on the size of the system and does not completely sample all states in the solvation process. The hydration enthalpy was calculated using the subtraction method for 4 different system sizes with side lengths of 20 Å, 21 Å, 25 Å, and 41 Å. Each system produced a different value of the hydration energy, with the energy becoming more negative as the system size increased, demonstrating the system size dependence of the method. Also, comparing these results to those of Stack (2009), both

using the same FF, but different systems sizes, yielded different values of the hydration enthalpy.

Subtracting the potential energy of the target state (the solvated ion) from the reference state (bulk water) does not include all the energetic contributions of the solvation process. Solvating an ion is the process of inserting an ion from a fixed position in an ideal gas into a fixed position in a solvent (Marcus, 1985). The subtraction technique does not take into account the energy of the formation of the solvation sphere during the introduction of the ion. This inaccuracy is overcome using perturbation theory by gradually turning off the Van der Waals and electrostatic interactions of the ion. Calculating the difference in energy in stages as the ion is gradually removed from solution samples all the states of the solvation process.

Subsequent free energy perturbation (FEP) calculations (See section 2.7.2) are performed on the barium, strontium, and sulfate force fields to obtain a more accurate estimate for the hydration energy (Chipot and Pohorille, 2007; P. Raiteri, Pers. Comm.). The FEP calculations produced the following values of the hydration Gibbs free energy for the aqua ions: barium is -1188 kJ/mol, 5 % less negative than the experimental result of -1250 kJ/mol (Marcus, 1991); strontium is -1341 kJ/mol, 3 % less negative than the experimental result of -1380 kJ/mol (Marcus, 1991); and sulfate is -968 kJ/mol, 10 % less negative than the experimental result of -1080 kJ/mol (Marcus, 1991). This study is instructive in that the correct hydration structure was attained for the aqueous ions, but two methods of determining the energies yielded values with up to 10 % error. The subtraction method's results show an overestimation of the hydration energies and the FEP method shows an underestimation. Underestimated values are more consistent with

the results as will be discussed below. This demonstrates that great care needs to be taken when calculating thermodynamic quantities from computational studies to compare to experimental values.

3.2 Potential of Mean Force Profiles for Ion-Pairs

$W(r)^{eff}$ profiles (Figure 3.2) were calculated out to 14 Å to capture of all salient features and energy barriers (Table 3.2). We found a succession of local maxima representing the bounds of the different ion-pair species described by the Eigen mechanism (MD snapshots of each ion-pair species are shown in Figure 3.3). Each system shows a CIP2 around 3.3 Å, though it is much more prominent for $BaSO_{4(aq.)}$, a CIP1 around 3.8 Å, a SHIP ranging from 6 Å to 7 Å, a SSIP ranging from 8 Å to 11 Å, and free ions (FI) exist after the cut-off value, R, (Ciccotti et al., 1989) which was chosen to be 11 Å for both systems under study, as justified below.

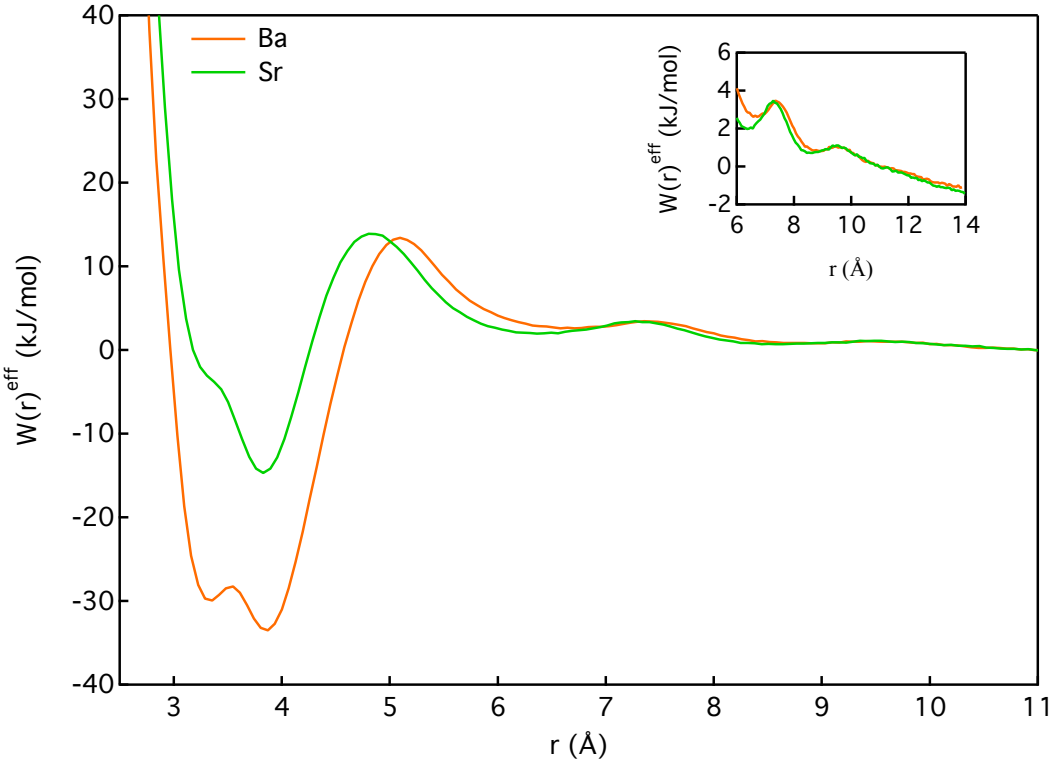

Figure 3.2 Normalized effective potential of mean force profiles for $BaSO_{4\,(aq.)}$ and $SrSO_{4\,(aq.)}$ ion-pairs. The inset is a magnification showing the FI to SSIP and SSIP to SHIP energy barriers and that there are no more significant features past 11Å.

Table 3.2: Energy Barrier Heights in kJ/mol for Different Ion-Pair Reactions

	CIP2|CIP1		CIP1|SHIP		SHIP|SSIP		SSIP|FI	
	→	←	→	←	→	←	→	←
$BaSO_4$	1.72	5.28	46.92	10.80	0.85	2.68	0.28	1.13
$SrSO_4$	-	-	28.58	11.93	1.49	2.76	0.41	1.12

→ represent dissociation reactions and ← represent association reactions

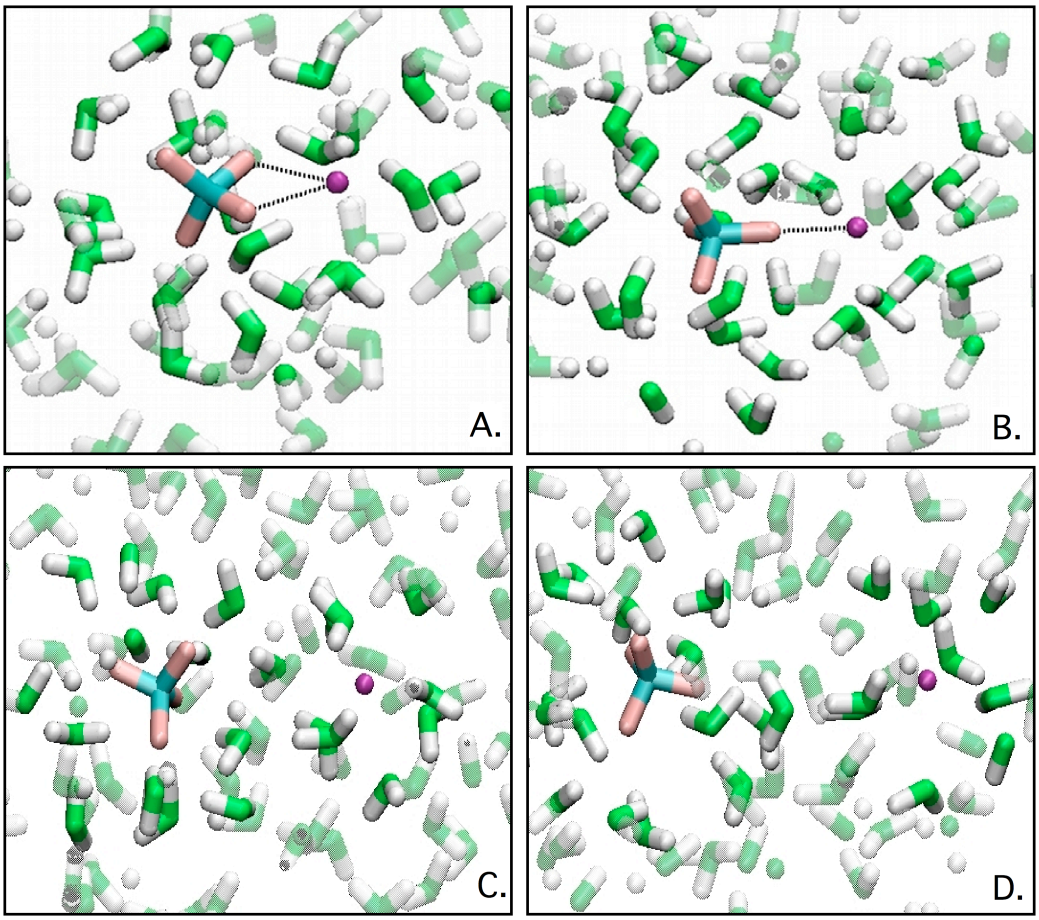

Figure 3.3 MD snapshots of four different ion-pairs described by the Eigen mechanism. The local solvation structure is highlighted by dimming all waters beyond 5 Å. Maroon atoms are the divalent cations, light blue is sulfur, orange is the oxygens on the sulfate, green is oxygens on water, and white are hydrogens. A. Bidentate contact ion-pair (CIP2). B. Monodentate contact ion-pair (CIP1). C. Solvent shared ion-pair (SHIP), interior waters are shared. D. Solvent seperated ion-pair (SSIP), showing two complete solvation shells.

The choice of the cut-off value, the division between FI and SSIP, has a significant effect on the resulting association constant (Figure 3.4). What constitutes the division between free ions and solvent separated ions is still a subject of debate (see Marcus & Hefter, 2006 for a review) and this study follows the approach of others (Guárdia et al., 1991; Chialvo et al., 1995; Larentzos and Criscenti, 2008; Matthews and Naidoo, 2010) by setting the potential of mean force at a reference distance, $W(r_0)$, equal to the purely Coulombic interaction between the ions at that distance by equating the

PMF at r_0 equal to Coulomb's law. This approach assumes that beyond r_0 the only effect the ions have on one another, if any, is long-range electrostatic interactions (Guárdia et al., 1991; Chialvo et al., 1996; Matthews and Naidoo, 2010).

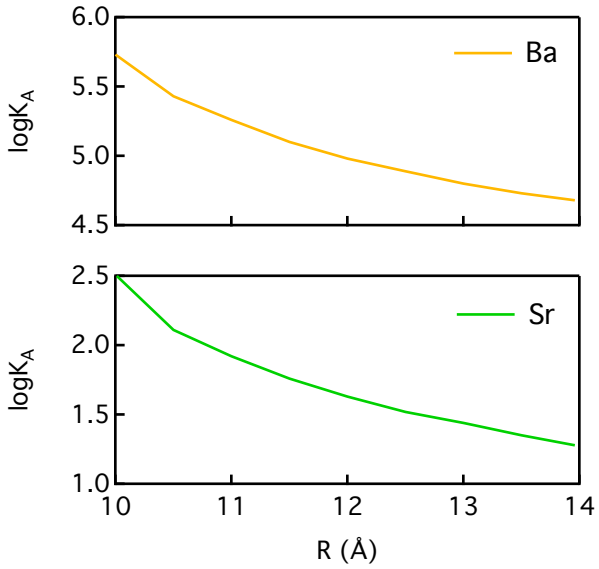

Figure 3.4 Association constant plotted as a function of the cut-off distance.

The choice of an 11 Å cut-off is valid for several reasons: One, past 11 Å the $W(r)^{eff}$ profile plateaus (Figure 3.2 inset), remaining featureless, indicating there are no more barrier-producing interactions. Two, neutron diffraction studies and quantum chemical calculations of ion solvation have demonstrated that the short-range water-water self-interaction forces overcome the ion-ion long-range electrostatic forces beyond the second shell for divalent cations and the first shell for anions (Asthagiri et al., 2004; Collins et al., 2007). For the ions to pair and become a distinct kinetic entity, they must be within each others' second or first solvation shell where the ions' short-range chemical forces dominate the reaction; the sum of these shell distances is within 11 Å for both $BaSO_{4(aq.)}$ and $SrSO_{4(aq.)}$ (Asthagiri et al., 2004; Collins et al., 2007). Three, the calculated Coulombic interactions at the reference distance are minimal, with a value

<0.7 J/mol (using the experimental dielectric constant for water at 25 °C of 78.2 (Marcus, 1985)), reinforcing point two. And four, the Bjerrum length, which is a theoretical maximum separation distance between two ions where they can still be considered paired, is calculated to be 11.16 Å for symmetrical divalent ion-pairs using the experimental dielectric constant for water (Marcus, 1985). The Bjerrum distance is found by calculating the probability that two ions will be at a certain separation distance; the distance at which the probability is a minimum is q_B (Marcus and Hefter, 2006):

$$q_B = q_i q_j e^2 / 2\varepsilon k_B T \tag{3.1}$$

where q_i is the charge on ion i, e is the fundamental charge, ε is the relative permittivity of the medium, k_B is Boltzmann's constant and T is the absolute temperature. This length is often used for the separation distance tolerance in conductance measurements (Marcus and Hefter, 2006).

The cut-off effect on the association constant raises an interesting point about what experimental cut-off the computational cut-off should be compared to. Fennell et al. (2009) raised the same question when comparing computational K_A values of alkali halide pairs to ones derived from conductance experiments and note in their investigation that the K_A values from experiment show a dependence on the separation distance tolerance (Duer et al., 1976; Marcus and Hefter, 2006). Hence, a more consistent definition for the separation distance or cut-off between free ions and solvent separated ion-pairs is needed to accurately compare simulation to experiment (Fennell et al., 2009). A better cut-off for experimentalist and theorists alike would come from an accepted consistent definition for the distance a pair of ions begins to act as a kinetically distinct species.

Analyzing the effective PMF profiles revealed a relationship between the ions' solvation and the energy barriers to association. There is an increase in the energy barrier height during association with the greatest barrier being the SHIP to CIP1 transition with a value of 11 kJ/mol for barium and 12 kJ/mol for strontium. As the ions associate, each stage of association expels more water molecules coordinated by the ions, corresponding to an increase in the free energy of interaction. Figure 3.5 demonstrates how the CN of each cation decreases during association, showing a step-wise descent associated with the formation of different ion pair species. The steps (or changes in slope in Figure 3.5) occur at the transition states that mark the dividing point between the different ion-pairs (Figure 3.2), where the steps at 5 Å and 3.5 Å are the formation of the CIP1 and CIP2, respectively. The largest dehydration step occurs at 5 Å corresponding to largest energy barrier. The difference in hydration of each cation can also be seen in Figure 3.5, which arises out of their different hydration energy (or charge density). These properties will help explain the different behavior observed between the two cations.

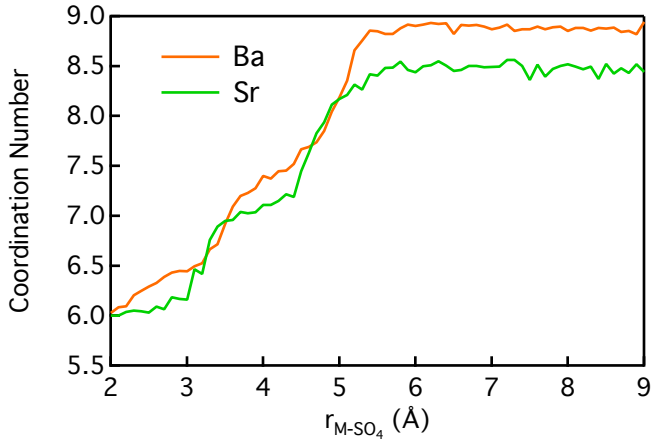

Figure 3.5 Calculated coordination number plotted against the cation-anion separation distance. Changes in slope at 5Å and 3.5Å corespond to approximate locations of transition states for CIP species.

Comparing barium to strontium, there is a positive relationship between charge density and the free energy of association for all ion-pair species. The cation with the higher charge density (strontium) shows greater energy barriers for the formation of all its ion-pair species. This is also reported in divalent metal-sulfate complexes (Matthews and Naidoo, 2010) and alkaline-earth metal chloride complexes (Larentzos and Criscenti, 2008). This reinforces the idea that the reactivity of an ion is controlled to a large extent by its hydration energy; as the charge density increases so does the hydration energy and the barriers to complex formation. An exception is the FI to SSIP transition, where the barriers for Ba^{2+} and Sr^{2+} are observed to be equivalent in this study.

The relative stability of each contact ion-pair is also a function of the cations' charge density. The well depth (i.e. local minimum in the PMF) of a mono-dentate complex (CIP1) increases with decreasing charge density, with barium favoring complexation with sulfate by 18 kJ/mol. This can be explained to be a result of barium's higher CN; it must therefore expel more waters (Figure 3.5) to dissociate. A CIP2 is also observed for both systems' though not as prevalent in strontium and the CIP2 only appears as a shoulder in the strontium PMF. The barium CIP2, however, shows a definite stability with a barrier of 5 kJ/mol, demonstrating again a greater stability with lower charge density.

The emergence of a bi-dentate complex (CIP2) with decreasing charge density is consistent with other studies of oxyanion ion-pairs as well. Divalent-metal nitrate complexes (Xu et al., 2008) show a CIP2 complex for Ca, Sr, and Pb, but no indication of a CIP2 for the smaller Mg ion. Another study on sulfate complexes (Matthews and Naidoo, 2010) shows $CaSO_4$ forms a bidentate complex, while smaller divalent ions Mg,

Mn, Co, Cu, Fe, Ni, and Zn maintain a monodentate conformation. Divalent metal carbonate and bicarbonate complexes also show this trend in a recent first principles MD study (Di Tommaso and de Leeuw, 2010). The free energy profiles were not computed for the (bi-)carbonate species, but the radial distribution function profiles do show that the larger ions studied (Ca^{2+} and Sr^{2+}) can form relatively stable bidentate complexes. The prevalence of a stable bidentate oxyanion complex suggests it may be an important step in mineral and nano-particle nucleation.

3.3 Association Constants from Potential of Mean Force Profiles

The logarithm of the association constants for $BaSO_{4(aq.)}$ and $SrSO_{4(aq.)}$ ion pair reactions are calculated (Table 3.3) from the PMF profiles and yield values of 5.26 and 1.92, respectively. Our $BaSO_{4(aq.)}$ result is 2.5 orders of magnitude greater than the current literature values of 2.72 (Felmy et al., 1990) and 2.26 (Monnin, 1999). This difference may be to an error in the hydration energy, which diminishes the strength of the Ba-OH_2 interactions. The strontium association constant on the other hand agrees well with the current literature value of 1.86 (Felmy et al., 1990). Although, the FF used has an incorrect value for the hydration energies (all aqua species are shown to be from 3-10 % under-hydrated), which explains why our values for the association constants are higher then the current literature values, it is suggested that the errors in the hydration free energies scale with the size of the ion. This would explain why a similar error in the hydration energy can have a different effect for each cation. Also, the results illustrate that a small error in the hydration enthalpy (or free energy) can have a large impact on the dynamics of the system.

Table 3.3: Calculated logK Values for Ion-Pairing

		Calculated	Exp.	Reference
$BaSO_{4(aq.)}$	K_A	5.26	2.72, 2.26	Felmy, 1990; Monnin, 1999
	K_1	-0.05	-	
	K_2	-0.39	-	
	K_3	5.61	-	
	K_4	-0.62	-	
$SrSO_{4(aq.)}$	K_A	1.92	1.86, 2.29	Felmy, 1990; Reardon & Armstrong, 1987
	K_1	0.05	-	
	K_2	-0.35	-	
	K_3	2.22	-	

The calculated equilibrium constants for the intermediate species (Table 3.3) are used to determine the relative abundances of the different ion-pairs of the system. The non-CIP species for $BaSO_{4(aq.)}$ represents 0.0007 % of the total $BaSO_{4(aq.)}$ with twice the amount of SSIP than SHIP. The CIP1 complex represents 81 % of the total and the CIP2 complex makes up the remaining 19 %. For $SrSO_{4(aq.)}$ the non-CIP represent 2 % of the total $SrSO_{4(aq.)}$ also with twice the amount of SSIP than SHIP and the CIP1 species makes up the remaining 98 %. The shoulder around 3.3 Å in the $SrSO_{4(aq.)}$ PMF did not permit the calculation of an equilibrium constant for the Sr CIP2 species. The small amount of non-CIP species in the system is consistent with the underestimation of the hydration energy and over-binding the association.

The speciation calculations can shed light on the molecular processes driving the association reaction. The overall association constant is dominantly controlled by the formation of the CIP1 species for both reactions because it has the highest energy barrier, accounts for the largest amount of pairs, and thus represents the rate-limiting step for both cases. The speciation calculations show that neglecting the non-CIP from the

evaluation of the overall association constant can produce an error of several percent for $SrSO_{4(aq.)}$. It is likely that non-CIP also affect the KA for $BaSO_{4(aq.)}$. More accurate hydration energy calculations will be necessary to confirm this. At very high concentrations (i.e. brines, hyper-saline lakes) the amount of CIP2 may become dominant (Larentzos and Criscenti, 2008).

3.4 Water Residence Times for Free and Paired Ions

The residence time, τ, of a water in the first shell of a free and paired Ba^{2+} and Sr^{2+} ion (Table 3.5) is calculated using the Reactive Flux (RF) method (Chandler, 1978). The $W(r)^{eff}$ profiles and corresponding radial distribution functions for Ba^{2+} and Sr^{2+} can be found in Figures 3.6 and 3.7 for free and paired ions respectively. The plots are virtually identical except for a small peak around 7.5 Å in Figure 3.7 corresponding to the first water shell opposite the sulfate from the cation. Plots of the transmission coefficients are in Figure 3.8.

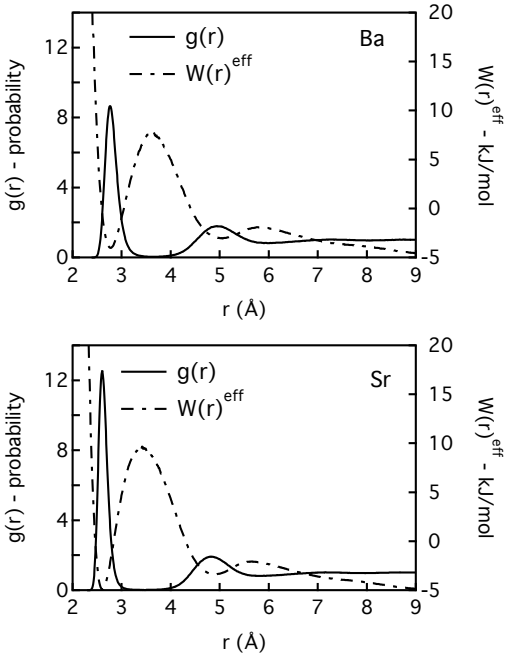

Figure 3.6 Radial distribution functions with corresponding effective potential of mean force profiles for barium (top) and strontium (bottom) used in the reactive flux calculations.

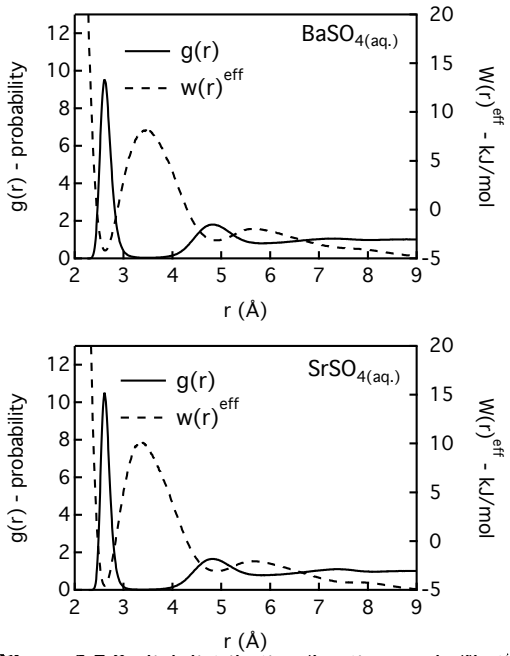

Figure 3.7 Radial distribution functions and effective potential of mean force profiles for barite (top) and celestite (bottom) contact ion pairs.

A residence time of 195 ps was obtained for free Ba^{2+}. This is much greater than a QM/MM result of 18 ps (Hofer et al., 2005) and a MD value of 14.6 ps (Larentzos & Criscenti, 2008). A residence time of 221 ps was obtained for free Sr^{2+}. This is also significantly higher than reported QM/MM values of 45 ps (Hofer et al., 2006) and two MD values of 43.1 ps (Larentzos & Criscenti, 2008) and 80 ps (Kerisit & Liu, 2010). The only experimental values for the rate constant of water exchange on Ba^{2+} or Sr^{2+} have been obtained by IQENS (Inelastic Quasi Elastic Neutron Scattering) or deduced from ligand exchange experiments, both estimate a value between 10^{9}-10^{10} s^{-1} for both ions, which is equivalent to a residence time of 100-1000 ps (Helm & Merbach, 1999; 2005). Our water exchange values are higher than other computational studies but within the experimentally determined range. Most importantly is that our model maintains the

relationship of Sr^{2+} having a longer residence time than for Ba^{2+} (Hofer et al., 2005, 2006; Larentzos and Criscenti, 2008) continuing the positive correlation between charge density and residence time.

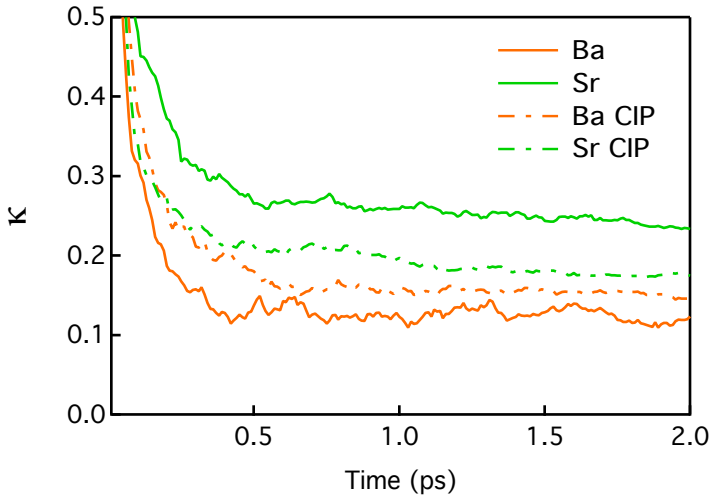

Figure 3.8 Transmission coefficients of free (solid) and paired (dashed) barium and strontium.

Table 3.4: Results from Reactive Flux Calculations

	k^{TST} (s^{-1})	κ	k_{H2O} (s^{-1})	τ (ps)	Comp. Ref. (ps)	Exp. Ref. (ps)
Ba^{2+}	4.36×10^{10}	0.12	5.12×10^{9}	195	18[a]	100-1000[d]
Sr^{2+}	1.97×10^{10}	0.23	4.52×10^{9}	221	45[b], 80[c]	100-1000[d]
$BaSO_{4(aq.)}$	2.19×10^{10}	0.15	3.23×10^{9}	310		
$SrSO_{4(aq.)}$	1.05×10^{10}	0.18	1.86×10^{9}	538		

[a]Hofer, 2005. [b]Hofer, 2006. [c]Kerisit and Liu, 2010. [d]Helm and Merbach, 2005.

The residence time of a water in the first shell of the cation in a CIP for both systems is also calculated. Sulfate complexation increases τ for Ba^{2+} and Sr^{2+} by factors of 1.6 and 2.4, respectively (Table 3.4). The transmission coefficients (Figure 3.8) indicate that the solvation structure has a reduced effect on the reaction progress for celestite, but an increased effect on the reaction progress for barite. Because the k^{TST} is

reduced more for $BaSO_{4(aq.)}$ than $SrSO_{4(aq.)}$, the increased effect of the solvation structure does not change the relationship observed between charge density and the residence times for the complexes. This result of sulfate increasing the residence time for each cation may be a steric effect from the sulfates physical proximity to the cations. These results also show that the complexation effect of sulfate increases with increasing charge density of the cation.

The reactive flux method is sensitive to the choice of the transition state configuration as well as to the hydration energy of the species, as that determines the energy surface. Errors could arrive from poorly chosen transition state configurations (Stack and Rustad, 2007), the effect the constraints have on the water orientation and dynamics, and poor hydration energies. This estimate can be improved with correcting the hydration energy as mentioned above and finding an alternative method of constraining the system.

To look at the effect the constraints have on the systems dynamics a residence time correlation function (Impey et al., 1983) is employed. The residence times from the correlation function for free Ba^{2+} and Sr^{2+} are 82 ± 9 ps and 125 ± 27 ps, respectively. These are faster than the results obtained from the RF technique, yet still longer than other computational studies. Regardless, the qualitative relationship between the residence time and the charge density is still observed.

Complexed Ba^{2+} and Sr^{2+} have residence times of 147 ± 26 ps and 146 ± 17 ps, respectively from the correlation function. The range in the fits for the correlation function make it difficult to determine if the sulfate's effect does increase with increasing

charge density, but it is shown that in both techniques; sulfate complexation increases the residence time of water around each cation.

CHAPTER 4: CONCLUSIONS

4.1 Conclusions

Molecular dynamics was used to examine ion-pair formation of barium and strontium with sulfate. The overall association constant, K_A, and individual equilibrium constants, K_i, for each reaction as described by the Eigen mechanism were also calculated and this study marks the first computational estimates of these values. The association constant for $BaSO_{4(aq.)}$ is 2.5 orders of magnitude higher than current literature values; this is attributed to be the result of an error in the hydration energy estimation. The association constant for $SrSO_4$ is similar to the value obtained previously by Felmy et al. (1990).

Several relationships between the charge density (or hydration energy) and the dynamics of the association are observed. As charge density increases (hydration energy becomes more positive) the free energy of association (i.e. complex formation) increases, creating higher energy barriers for the strontium pairs than the barium. The stability of the different CIP species is also seen as a function of the charge density. The Ba CIP1 species is 18 kJ/mol more stable than the Sr CIP1 and the Ba CIP2 is 5 kJ/mol more stable than the Sr CIP2. The CIP2 for Sr appears only as a shoulder in the Sr PMF suggesting it is unstable in this model. The Ba CIP2 complex accounts for nearly 19% of the total ion-pairs in the system, indicating that the presence of the CIP2 increases with increasing charge density. This same relationship is observed in nitrate complexes (Xu et al., 2008) and other sulfate complexes (Matthews and Naidoo, 2010).

Additionally, the change in CN with the cation-anion separation distance shows a slope change at the transition states for the CIP1 and CIP2 species. This reveals the difference in the solvation of the two CIP species; that at the transition state the configuration is unstable and rapidly progresses to a more stable solvation structure. A detailed analysis of the CN vs. $r_{M\text{-}SO4}$ relationship provides information about the transition states structures for CIP formation.

The calculated water residence times were higher than current literature values from other computational studies, but within the predicted experimental values from IQENS and ligand substitution (Helm and Merbach, 1999; 2005). The two techniques used to compute the residence times yielded consistent results. The residence time of a water around a free Ba^{2+} ion is 82 ± 9 ps with the correlation function and 195 ps using RF. For free Sr^{2+} the water residence time is 125 ± 27 ps with the correlation function and 221 ps using RF. For complexed Ba^{2+} the water residence time is 147 ± 26 ps with the correlation function and 310 ps with RF. For complexed Sr^{2+} the water residence time is 146 ± 17 ps with the correlation function and 538 ps using RF. Both methods reveal that sulfate complexation increases the water residence time, this is explained to be the result of a steric effect from the sulfate on the cations and coordinated waters.

4.2 Future Work

Follow-up work to this study would consist of a reparameterization of the FF by FEP calculations to ensure a correct free energy of the aqua ions and also to calculate the solvation free energy of the complex with FEP methods similar to the approach of Matthews and Naidoo (2010). Beyond this I would like to extend the study of aqua ions to nano-particle or colloid formation and the energy barriers and kinetics associated with

these phenomena. Along this line of thought a long-term goal is to use MD to investigate mineral nucleation in solution.

Dielectric relation spectroscopy (DRS) could be employed to complement the simulations starting with reevaluating the barite and celestite association constants obtained from solubility experiments. DRS is emerging as a powerful tool in studying aqueous complex formation (Buchner and Hefter, 2009) and offers an additional tool for geochemists to obtain equilibrium constants.

References

Asthagiri, D.; Pratt, L.R.; Paulaitis, M.E.; Rempe, S.B. Hydration structure and free energy of biomolecularly specific aqueous dications, including Zn2+ and first transition row metals. *Journal of the American Chemical Society* **2004**, 126, 1285-1289.

Burgess, J., *Ions In Solution*. Horwood, Chichester. **1999**.

Buchner, R.; Hefter, G., Interactions and dynamics in electrolyte solutions by dielectric spectroscopy. *Physical Chemistry Chemical Physics* **2009**, 11, 8984-8999.

Chandler, D. Statistical-mechanics of isomerization dynamics in liquids and transition-state approximation. *Journal of Chemical Physics* **1978,** 68 (6), 2959-2970.

Chandler, D. *Introduction to Modern Statistical Mechanics.* Oxford University Press. **1987**.

Chialvo, A. A.; Cummings, P. T.; Cochran, H. D.; Simonson, J. M.; Mesmer, R. E., Na+-Cl- ion-pair association in supercritical water. *Journal of Chemical Physics* **1995,** *103* (21), 9379-9387.

Chialvo, A. A.; Simonson, J. M., Aqueous Na+Cl- pair association from liquid like to steam like densities along near-critical isotherms. *Journal of Chemical Physics* **2003,** *118* (17), 7921-7929.

Chipot, C,; Pohorille, A., *Free Energy Calculations*. **2007**. Springer-Verlag, Berlin

Ciccotti, G.; Ferrario, M.; Hynes, J. T.; Kapral, R., Constrained molecular-dynamics and the mean potential for an ion-pair in a polar-solvent. *Chemical Physics* **1989,** *129* (2), 241-251.

Collins, K.D.; Neilson, G.W.; Enderby, J.E., Ions in water: characterizing the forces that control chemical processes and biological structure. *Biophysical Chemistry*, **2007**, (128), 95-104.

Cummings, P.T.; Stell, G., Statistical mechanical models of chemical-reactions analytic solution of models of A+B reversible AB in the percus-yevick approximation. *Molecular Physics* **1984,** 51(2), 253-287

Cygan, R. T., Molecular modeling in mineralogy and geochemistry. In *Molecular Modeling Theory: Applications in the Geosciences*, **2001**; Vol. 42, pp 1-35.

Di Tommaso, D.; de Leeuw, N.H., First Principles Simulations of the Structural and

Dynamical Properties of Hydrated Metal Ions Me2+ and Solvated Metal Carbonates (Me = Ca, Mg, and Sr), *Crystal Growth & Design* **2010**, 10(10), 4292-4302.

Drever, J.I., *The Geochemistry of Natural Waters*. Prentice Hall, 3rd Ed., **1997**

Duer, W.C.; Robinson, R.A.; Bates, R.G., Conductivity and ion-pairing of hydrogen-chloride in N-methylpropionamide at 25-degrees-C. *Journal of Solution Chemistry* **1976**, 5(11), 765-771.

Eigen, M.; Tamm, K., Schallabsorption in elektrolytlosungen als folge chemischer relaxation .2. messergebnisse und relaxationsmechanismen fur 2-2-wertige elektrolyte. *Zeitschrift Fur Elektrochemie* **1962,** 66 (2), 107-121.

Eyring, H., The activated complex in chemical reactions. *Journal of Chemical Physics* **1935,** *3* (2), 107-115.

Frenkel, D; Smit, B., *Understanding Molecular Simulation: From Algorithms to Applications,* 2nd Ed., Academic Press, **2002**.

Felmy, A.R.; Rai, D.; Amonette, E., The Solubility of Barite and Celestite in Sodium Sulfate: Evaluation of Thermodynamic Data. *Journal of Solution Chemistry* **1990,** 19 (2), 175-185.

Ghoufi, A.; Malfreyt, P., Calculations of the potential of mean force from molecular dynamics simulations using different methodologies: an application to the determination of the binding thermodynamic properties of an ion pair. *Molecular Physics*. **2006**, 104 (22), 3787-3799.

Grossfield, A.,"WHAM: the weighted histogram analysis method", Version 2.0.0, http://dasher.wustl.edu/alan/wham, accessed 6/23/2007

Guárdia, E.; Rey, R.; Padro, J. A., Potential of mean force by constrained molecular-dynamics - a sodium-chloride ion-pair in water. *Chemical Physics* **1991,** *155* (2), 187-195.

Hanor, J. S., Barite-celestine geochemistry and environments of formation. In *Sulfate Minerals - Crystallography, Geochemistry and Environmental Significance*, **2000**; Vol. 40, pp 193-275.

Hardy, J.A.;Simm, I, Low sulfate Seawater mitigates barite scale. *Oil & Gas Journal* **1996,** 94 (50), 64-67.

Hefter, G., When spectroscopy fails: The measurement of ion pairing. *Pure and Applied Chemistry* **2006,** *78* (8), 1571-1586.

Helm, L.; Merbach, A. E., Water exchange on metal ions: experiments and simulations. *Coordination Chemistry Reviews* **1999,** *187*, 151-181.

Helm, L.; Merbach, A. E., Inorganic and bioinorganic solvent exchange mechanisms. *Chemical Reviews* **2005,** *105* (6), 1923-1959.

Hoareau, G.; Monnin, C.; Odonne, F., A study of celestine equilibrium in marine sediments using the entire ODP/IODP porewater database. *Geochimica et Cosmochimica Acta* **2010,** *74* (14), 3925-3937.

Hofer, T. S.; Randolf, B. R.; Rode, B. M., Sr(II) in water: A labile hydrate with a highly mobile structure. *Journal of Physical Chemistry B* **2006,** *110* (41), 20409-20417.

Hofer, T. S.; Rode, B. M.; Randolf, B. R., Structure and dynamics of solvated Ba(II) in dilute aqueous solution - an ab initio QM/MM MD approach. *Chemical Physics* **2005,** *312* (1-3), 81-88.

Hofer, T. S.; Tran, H. T.; Schwenk, C. F.; Rode, B. M., Characterization of dynamics and reactivities of solvated ions by ab initio simulations. *Journal of Computational Chemistry* **2004,** *25* (2), 211-217.

Impey, R. W.; Madden, P. A.; McDonald, I. R., Hydration and mobility of ions in solution. *Journal of Physical Chemistry* **1983,** *87* (25), 5071-5083.

Iskrenova-Tchoukova, E.; Kalinichev, A. G.; Kirkpatrick, R. J., Metal Cation Complexation with Natural Organic Matter in Aqueous Solutions: Molecular Dynamics Simulations and Potentials of Mean Force. *Langmuir* **2010,** *26* (20), 15909-15919.

Jang, Y. H.; Chang, X. Y.; Blanco, M.; Hwang, S. G.; Tang, Y. C.; Shuler, P.; Goddard, W. A., The MSXX force field for the barium sulfate-water interface. *Journal of Physical Chemistry B* **2002,** *106* (38), 9951-9966.

Kerisit, S; Rosso, K.M., Transition path sampling of water exchange rates and mechanisms around aqueous ions. *The Journal of Chemical Physics* **2009**, 131 (11), 114512-114515.

Kerisit, S.; Liu, C. X., Molecular simulation of the diffusion of uranyl carbonate species in aqueous solution. *Geochimica et Cosmochimica Acta* **2010,** *74* (17), 4937-4952.

Kumar, S.; Bouzida, D.; Swendsen, R. H.; Kollman, P. A.; Rosenberg, J. M., The weighted histogram analysis method for free-energy calculations on biomolecules .1. the method. *Journal of Computational Chemistry* **1992,** *13* (8), 1011-1021.

Larentzos, J. P.; Criscenti, L. J., A Molecular Dynamics Study of Alkaline Earth Metal-Chloride Complexation in Aqueous Solution. *Journal of Physical Chemistry B* **2008,** *112* (45), 14243-14250.

Levitt, M.; Hirshberg, M.; Sharon, R.; Laidig, K. E.; Daggett, V., Calibration and testing of a water model for simulation of the molecular dynamics of proteins and nucleic acids in solution. *Journal of Physical Chemistry B* **1997,** *101* (25), 5051-5061.

Marcus, Y., *Ion Solvation*. John Wiley & Sons, London. **1985**

Marcus, Y., Thermodynamics of solvation of ions. Part 5-Gibbs free energy of hydration at 298.15 K. *Journal of the Chemical Society – Faraday Transactions* **1991,** 87(18), 2995-2999.

Marcus, Y.; Hefter, G., Ion pairing. *Chemical Reviews* **2006,** *106* (11), 4585-4621.

Matthews, R. P.; Naidoo, K. J., Experimentally Consistent Ion Association Predicted for Metal Solutions from Free Energy Simulations. *Journal of Physical Chemistry B* **2010,** *114* (21), 7286-7293.

Mayo, S. L.; Olafson, B. D.; Goddard, W. A., Dreiding - a generic force-field for molecular simulations. *Journal of Physical Chemistry* **1990,** *94* (26), 8897-8909.

McQuarrie, D., Statistical Mechanics, Harper & Row, New York, **1976.**

Monnin, C.; Jeandel, C.; Cattaldo, T.; Dehairs, F., The marine barite saturation state of the world's oceans. *Marine Chemistry* **1999,** *65* (3-4), 253-261.

Ohtaki, H.; Radnai, T., Structure and dynamics of hydrated ions. *Chemical Reviews* **1993,** *93* (3), 1157-1204.

Parkman, R.H.; Charnok, J.M.; Livens, F.R.; Vaughan, D.J., A study of strontium ions in aqueous solution with the surface of calcite and kaolinite. *Geochimica et Cosmochimica Acta*. **1998**, 62 (9), 1481-1492.

Persson, I.; Sandstrom, M.; Yokoyama, H.; Chaudhry, M., structure of the solvated strontium and barium ions in aqueous, dimethyl-sulfoxide and pyridine solution, and crystal-structure of strontium and barium hydroxide octahydrate. *Zeitschrift Fur Naturforschung Section a-a Journal of Physical Sciences* **1995,** *50* (1), 21-37.

Plimpton, S., Fast parallel algorithms for short-range molecular-dynamics. *Journal of Computational Physics* **1995,** *117* (1), 1-19.

Pottel R.; Hollar J.; Kaatze U.; Multi-step association of cation and anions. The Eigen-Tamm mechanism some decades later. In Kurz T.; Parlitz U.; Kaatze U.; Eds.

Oscillations, Waves, and Interactions Universitätsverlag Göttingen, Germany. **2007,** 333-366.

Raiteri, P.; Gale, J.D., Water Is the Key to Nonclassical Nucleation of Amorphous Calcium Carbonate. *Journal of the American Chemical Society* **2010,** 132, 17623-17634

Reardon, E. J.; Armstrong, D. K., Celestite (SrSO4(s)) solubility in water, seawater and NaCl solution. *Geochimica et Cosmochimica Acta* **1987,** *51* (1), 63-72.

Rey, R.; Hynes, J. T., Hydration shell exchange kinetics: An MD study for Na+(aq). *Journal of Physical Chemistry* **1996,** *100* (14), 5611-5615.

Richens, D.T., *The Chemistry of Aqua Ions: Synthesis, Structure and Reactivity: A Tour Through the Periodic Table of the Elements*. Wiley, **1997**.

Richter F.M.; Models for the coupled Sr-sulfate budget in deep-sea carbonates. *Earth and Planetary Sciences Letters* **1996**, 141, 199-211.

Roux, B., The calculation of the potential of mean force using computer-simulations. *Computer Physics Communications* **1995,** *91* (13), 275-282.

Ryckaert, J. P., special geometrical constraints in the molecular-dynamics of chain molecules. *Molecular Physics* **1985,** *55* (3), 549-556.

Schenter, G. K.; Garrett, B. C.; Truhlar, D. G., Generalized transition state theory in terms of the potential of mean force. *Journal of Chemical Physics* **2003,** *119* (12), 5828-5833.

Smith, W.; Forester, T.R., DL_POLY_2.0: A general purpose parallel molecular dynamics simulation package. *Journal of Molecular Graphics* **1996,** 14(3), 136-141.

Soper, A. K.; Phillips, M. G., A new determination of the structure of water at 25-degrees-c. *Chemical Physics* **1986,** *107* (1), 47-60.

Spångberg, D.; Rey, R.; Hynes, J. T.; Hermansson, K., Rate and mechanisms for water exchange around Li+(aq) from MD simulations. *Journal of Physical Chemistry B* **2003,** *107* (18), 4470-4477.

Stack, A.G. Molecular Dynamics Simulations of Solvation and Kink Site Formation at the {001} Barite-Water Interface. *Journal of Physical Chemistry C* **2009**, 113 (6) 2104-2110.

Stack, A. G.; Rustad, J. R., Structure and dynamics of water on aqueous barium ion and the {001} barite surface. *Journal of Physical Chemistry C* **2007,** *111* (44), 16387-16391.

Vchirawongkwin, V.; Rode, B. M.; Persson, I., Structure and dynamics of sulfate ion in aqueous solution - An ab initio QMCF MD simulation and large angle X-ray scattering study. *Journal of Physical Chemistry B* **2007,** *111* (16), 4150-4155.

Wigner, E., The transition state method. *Transactions of the Faraday Society* **1938,** *34* (1), 29-40.

Xu, M.; Larentzos, J. P.; Roshdy, M.; Criscenti, L. J.; Allen, H. C., Aqueous divalent metal-nitrate interactions: hydration versus ion pairing. *Physical Chemistry Chemical Physics* **2008,** *10* (32), 4793-4801.

Yuan, M. D.; Todd, A. C.; Sorbie, K. S., Sulfate scale precipitation arising from seawater injection - a prediction study. *Marine and Petroleum Geology* **1994,** *11* (1), 24-30.